BIOTECHNOLOGY

Directed assembly of genetically engineered eukaryotic cells into living functional materials via ultrahigh-affinity protein interactions

Qikun Yi[1,2,3]†, Xin Dai[4,5]†, Byung Min Park[1], Junhao Gu[1], Jiren Luo[1], Ri Wang[1], Cong Yu[6], Songzi Kou[2,3,6], Jinqing Huang[4]*, Richard Lakerveld[1]*, Fei Sun[1,2,3]*

Engineered living materials (ELMs) are gaining traction among synthetic biologists, as their emergent properties and nonequilibrium thermodynamics make them markedly different from traditional materials. However, the aspiration to directly use living cells as building blocks to create higher-order structures or materials, with no need for chemical modification, remains elusive to synthetic biologists. Here, we report a strategy that enables the assembly of engineered *Saccharomyces cerevisiae* into self-propagating ELMs via ultrahigh-affinity protein/protein interactions. These yeast cells have been genetically engineered to display the protein pairs SpyTag/SpyCatcher or CL7/Im7 on their surfaces, which enable their assembly into multicellular structures capable of further growth and proliferation. The assembly process can be controlled precisely via optical tweezers or microfluidics. Moreover, incorporation of functional motifs such as super uranyl-binding protein and mussel foot proteins via genetic programming rendered these materials suitable for uranium extraction from seawater and bioadhesion, respectively, pointing to their potential in chemical separation and biomedical applications.

INTRODUCTION

Biological tissues or organs are remarkable multicellular materials that can self-grow, regenerate, evolve, and adapt. De novo design of these "living" materials has been unthinkable within traditional materials science. It is until recently that the convergence of synthetic biology and materials science has made it possible to create some engineered living materials (ELMs) that can recapitulate the natural ones to some extent (*1*, *2*). One typical example is to genetically or chemically reengineer some naturally occurring soft biomaterials such as bacterial biofilms (*1*, *2*). However, this approach has largely focused on the self-assembling biofilm proteins at the molecular level while exerting little control over the organization of cells. Although several other studies have demonstrated the controlled assembly of eukaryotic cells (e.g., yeasts or mammalian cells), often with the help of exogenous polymers, into tissue-like structures via DNA hybridization or click chemistry (*3*–*8*), these processes involved extensive chemical modifications, which might pose uncertainties for cellular fitness and biofunctionality. As the long-range organization of cells has been the hallmark of multicellular tissues and organs in higher organisms, the use of engineered cells as building blocks to construct high-order structures, while circumventing chemical modification, would add a new dimension to the design of ELMs (*9*, *10*).

"Ultrahigh-affinity" protein/protein interactions (PPIs) have often been used to assemble recombinant proteins into functional materials (*11*–*17*). For instance, SpyTag/SpyCatcher, a peptide/protein pair that is originally derived from a split bacterial adhesin domain, is capable of covalently stitching together protein molecules under mild physiological conditions, which has led to the creation of a number of uncommon protein architectures and materials (Fig. 1A) (*18*, *19*). Those noncovalent pairs, such as cohesin, X module/dockerin, the WW domain/its cognate proline-rich peptide, and the inactivated colicin E7 deoxyribonuclease/immunity protein 7 (CL7/Im7), can form strong physical interactions with dissociation constants (K_d) at low picomolar or even femtomolar, which have contributed to the formation of injectable hydrogels with shear-thinning behavior (*20*, *21*). The recently developed CL7/Im7, with an ultrahigh affinity (K_d ~10^{-14} to 10^{-17} M), has also provided a means to purify delicate protein complexes from biological systems (Fig. 1B). For materials design and synthesis, these PPI motifs can be readily introduced because of their genetic encodability and modularity. We envisioned that not only can biomolecules be assembled into macroscopic materials but also cells can serve as building blocks to construct high-order living materials. To accomplish this, the key is to endow the cells with the ability to form stable and specific intercellular interactions, the latter of which can be realized through the combined use of suitable protein chemistries and robust cell surface display systems.

Saccharomyces cerevisiae (baker's yeast) cells have been noted for their asexual cellular aggregation at a high cell density, a natural phenomenon also known as flocculation, when cells adhere reversibly to each other via the physical interactions between surface glycoproteins, leading to the formation of macroscopic aggregates during culturing (*22*). Inspired by the yeast cell aggregation, in this study, we accomplished controlled assembly of single-celled *S. cerevisiae* into highly stable, multicellular ELMs via genetically programmed intercellular interactions. The cells were engineered to produce and display ultrastrong PPI motifs such as SpyCatcher/SpyTag or CL7/Im7.

[1]Department of Chemical and Biological Engineering, The Hong Kong University of Science and Technology, Clear Water Bay, Kowloon, Hong Kong SAR, China. [2]Greater Bay Biomedical InnoCenter, Shenzhen Bay Laboratory, Shenzhen 518036, China. [3]Biomedical Research Institute, Shenzhen Peking University–The Hong Kong University of Science and Technology Medical Center, Shenzhen 518036, China. [4]Department of Chemistry, The Hong Kong University of Science and Technology, Clear Water Bay, Kowloon, Hong Kong SAR, China. [5]Laboratory for Synthetic Chemistry and Chemical Biology, Health@InnoHK, Hong Kong Science Park, Hong Kong SAR, China. [6]Department of Biology, School of Life Sciences, Southern University of Science and Technology of China, Shenzhen 518036, China.
*Corresponding author. Email: kefsun@ust.hk (F.S.); r.lakerveld@ust.hk (R.L.); jqhuang@ust.hk (J.H.)
†These authors contributed equally to this work.

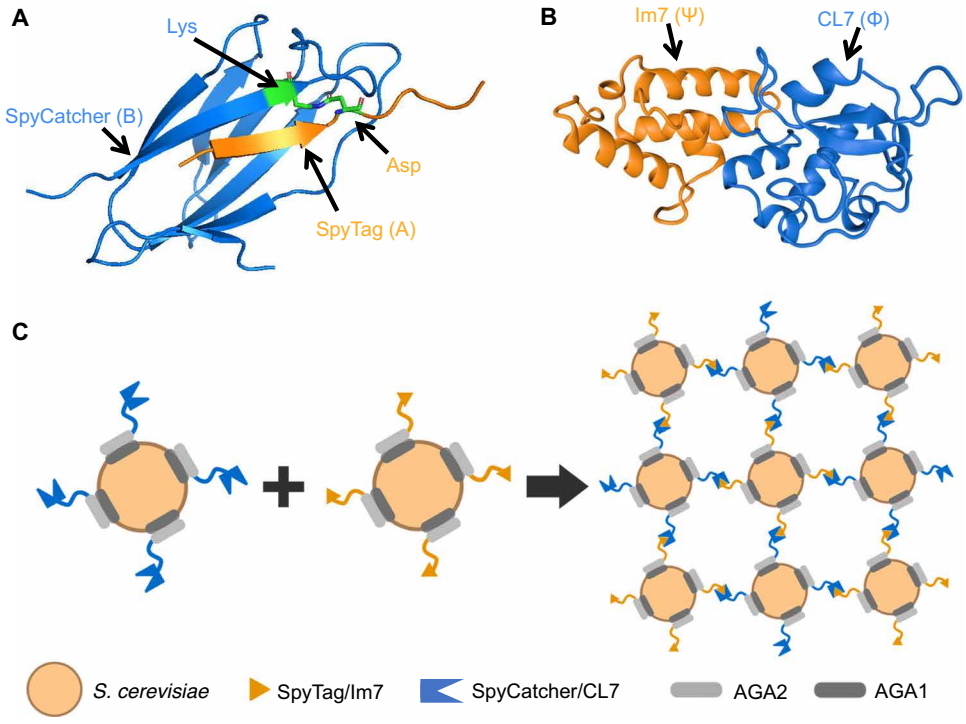

Fig. 1. Schematic showing the assembly of multicellular living material enabled by ultrahigh-affinity PPIs. (**A**) Structure of the SpyTag/SpyCatcher complex and the formation of isopeptide bond [Protein Data Bank identifier (PDB ID): 4MLI]. (**B**) Structure of the CL7/Im7 complex (PDB ID: 7CEI). (**C**) Assembly of *Saccharomyces cerevisiae* cells. AGA1 and AGA2 proteins enable the display of the target proteins, such as SpyTag, SpyCatcher, CL7, and Im7, on the cell surface. Intercellular PPIs assemble individual cells into networks.

Further introduction of functional motifs such as metalloproteins and underwater adhesive domains into these single-celled components gave rise to the corresponding emergent properties at the macroscopic material level. This study illustrates a simple strategy for creating functional living materials, which holds great promise for real-world challenges ranging from chemical separation to wound closure.

RESULTS AND DISCUSSION

Yeast surface display of ultrahigh-affinity binding partners

To achieve stable cell-to-cell conjugation, we chose two representative PPI partners—the covalent SpyTag/SpyCatcher that spontaneously forms a Lys-Asp isopeptide bond and the noncovalent, ultrahigh-affinity CL7/Im7 (Fig. 1, A and B). Yeast surface display was accomplished via the widely used AGA1/AGA2 system (*23*).

The genes encoding SpyTag, SpyCatcher, Im7, and CL7 were cloned into the pCTcon2 vector and then transformed into the *S. cerevisiae* strain EBY100 (*24*). The resulting yeast cells, denominated as *ScA*, *ScB*, *ScΦ*, and *ScΨ*, were expected to be able to produce and display the fusion proteins, AGA2-SpyTag, AGA2-SpyCatcher, AGA2-CL7, and AGA2-Im7, respectively, on their surfaces (Fig. 1C and table S1).

To confirm the expression and display of these proteins, we treated these cells, *ScA*, *ScB*, *ScΦ*, and *ScΨ*, correspondingly with the fluorescent proteins, SpyCatcher-elastin-like-protein (ELP)–enhanced green fluorescent protein (EGFP)–ELP-SpyCatcher, SpyTag-ELP-EGFP-ELP-SpyTag, Im7-ELP-EGFP-ELP-Im7, and CL7-ELP-EGFP-ELP-CL7 (table S2). These engineered cells, but not the wild-type ones, were labeled with EGFP efficiently, showing successful protein expression and surface display (Fig. 2).

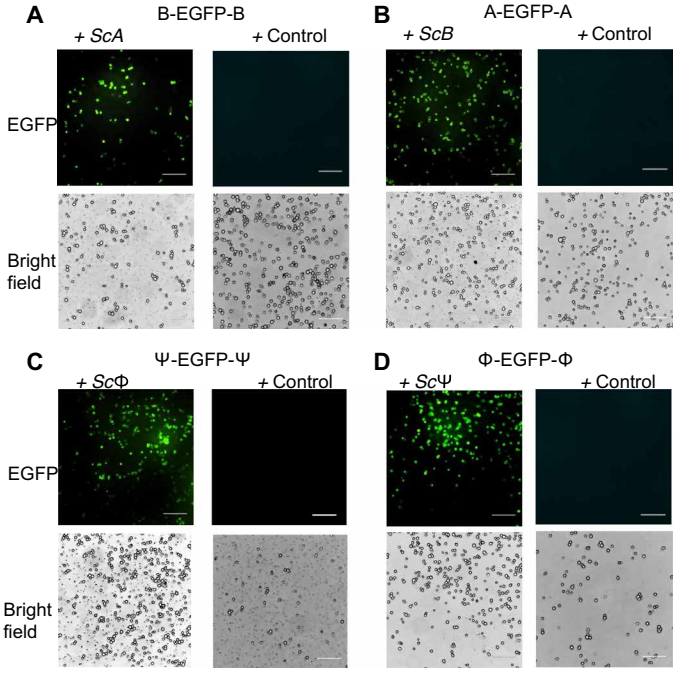

Fig. 2. Yeast surface display of interacting motifs confirmed by EGFP labeling. *S. cerevisiae* cells displaying SpyTag (*ScA*) (**A**), SpyCatcher (*ScB*) (**B**), CL7 (*ScΦ*) (**C**), and Im7 (*ScΨ*) (**D**) were labeled with SpyCatcher-ELP-EGFP-ELP-SpyCatcher (B-GFP-B), SpyTag-ELP-EGFP-ELP-SpyTag (A-GFP-A), Im7-ELP-EGFP-ELP-Im7 (Ψ-EGFP-Ψ), and CL7-ELP-EGFP-ELP-CL7 (Φ-EGFP-Φ), respectively. The yeast cells that did not display the proteins served as control. Scale bars, 50 μm.

Multicellular assembly at a high cell density

Being widely used to assemble biomolecules into high-order structures (*14*, *16*), genetically programmable PPIs may well be used to assemble larger mesoscopic objects like living cells into ELMs. Because of their natural tendency to adhere to each other at a high cell density, *S. cerevisiae* cells provide an ideal platform for achieving PPI-mediated ultrastable multicellular assembly while circumventing diffusion barriers. To test this hypothesis, we simply mixed the matched cell types, *ScA* + *ScB* and *ScΦ* + *ScΨ*, at an approximately 1:1 ratio and a cell density of ~2.0×10^8 per milliliter. To assess the cell-to-cell conjugation and also distinguish the two types of cells, the mixtures, *ScA* + *ScB* and *ScΦ* + *ScΨ*, were treated sequentially with the fluorescent proteins, SpyCatcher-ELP-Dronpa/SpyTag-ELP-mCherry-ELP-SpyTag and Im7-ELP-mCherry/CL7-ELP-EGFP-ELP-CL7, respectively. To avoid the undesirable reactions between the fluorescent proteins that may confound the cell labeling, we first treated the cell mixtures with the monovalent fluorescent proteins, SpyCatcher-ELP-Dronpa and Im7-ELP-mCherrry, to label *ScA* and *ScΦ*, respectively, followed by the other divalent ones, SpyTag-ELP-mCherry-ELP-SpyTag and CL7-ELP-EGFP-ELP-CL7, to label *ScB* and *ScΨ*; the other way around may doubly label *ScB* and *ScΨ*. The subsequent confocal microscopic imaging revealed that the matched pairs, *ScA* + *ScB* and *ScΦ* + *ScΨ*, led to multicellular clusters in numbers significantly larger than the mismatched pairs, *ScA* + *ScΦ*, *ScA* + *ScΨ*, *ScB* + ScΦ, and *ScB* + *ScΨ*, which suggest that the observed clustering is mainly driven by the specific interactions mediated by SpyTag/SpyCatcher and CL7/Im7 on the cell surfaces (Fig. 3).

Intercellular assembly controlled by optical tweezers

Optical tweezers are powerful, yet noninvasive tools for manipulating living cells (*25*). Their exquisite capabilities in force measurement also make it possible to quantitatively analyze intercellular interactions (*26*, *27*), so as to distinguish the engineered interactions (i.e., SpyTag/SpyCatcher or Im7/CL7) from the innate ones mediated by the natural glycoproteins such as flocculins. Figure 4A illustrates the way that we trapped a yeast cell in the microfluidic laminar flow chamber using a 1064-nm laser beam. Optically trapping two cells simultaneously with two laser beams allowed us not only to control the intercellular conjugation but also to quantify its strength by pulling the conjugate apart (Fig. 4B). When the matched cells were trapped and paired, strong intercellular interactions were observed (Fig. 4C and movies S1 to S10) (*28*, *29*), as the cells remained attached until the pulling forces reached 334.6 ± 20.1 and 335.0 ± 48.7 pN for *ScA* + *ScB* and *ScΦ* + *ScΨ*, respectively. Moreover, the conjugations between the matched cells, *ScA* + *ScB* and *ScΦ* + *ScΨ*, controlled by optical trapping proved to be robust by the consistent outcomes observed from at least 10 repeats (Fig. 4, D and E). By contrast, negligible interaction forces (<10 pN) were detected between the mismatched cells, *ScA* + *ScA* or *ScB* + *ScΦ*, confirming the essential roles of specific PPIs such as SpyTag/SpyCatcher and Im7/CL7 in the stable cell-to-cell conjugation (Fig. 4, D and E, and fig. S1). Together, these results demonstrated the feasibility of using optical trapping to delicately control and quantitatively assess the assembly of living cells, the latter of which further enabled us to differentiate the designed ultrahigh-affinity intercellular interactions from the innate weak ones.

Growth and proliferation of stable multicellular assemblies

Self-propagation is an important characteristic of living matter. To assess whether the multicellular assemblies were able to self-propagate

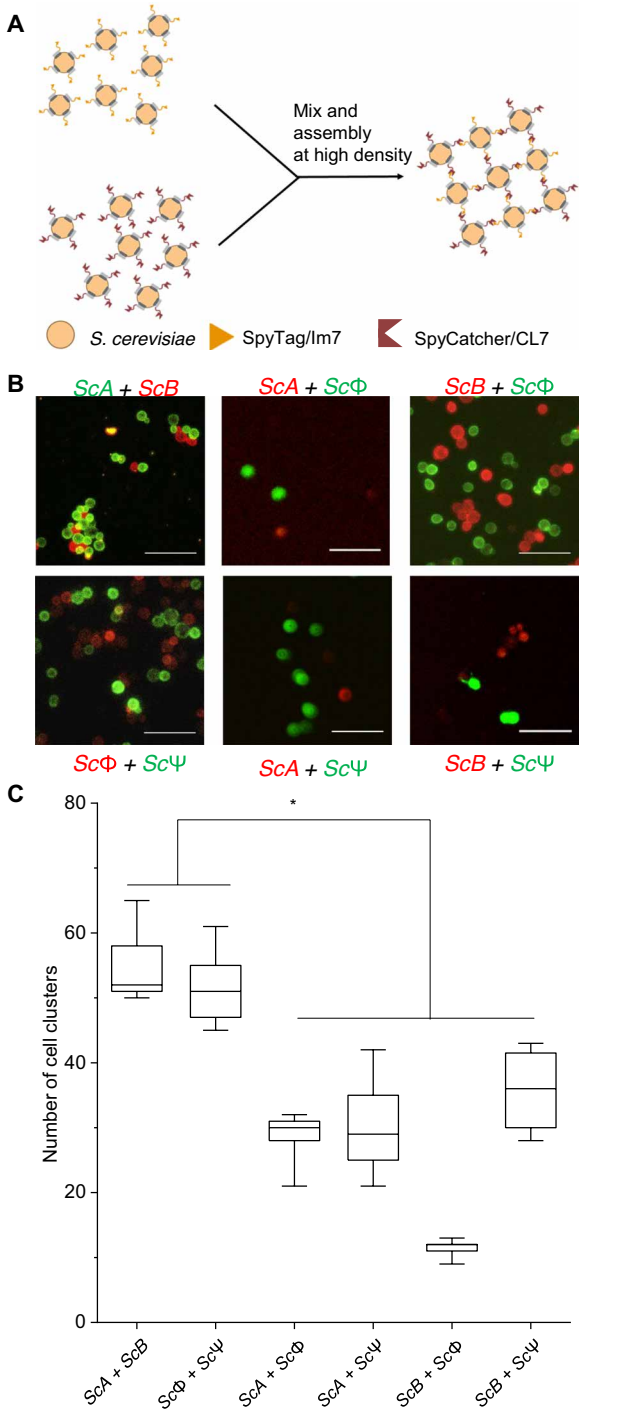

Fig. 3. Cell-to-cell conjugation mediated by surface-displayed SpyTag/SpyCatcher and CL7/Im7 at a high cell density. (**A**) Schematic showing the mixing and assembly process of the matched cell pairs at high density. (**B**) Representative micrographs of the matched pairs, *ScA* + *ScB* and *ScΦ* + *ScΨ*, and the mismatched pairs, including *ScA* + *ScΨ*, *ScB* + *ScΨ*, *ScΦ* + *ScA*, and *ScΦ* + *ScB*. Scale bars, 25 μm. (**C**) Number of multicellular clusters that consist of ≥3 cells. The two-sample *t* test was used. Data are presented as means ± SD ($n = 5$). *$P < 0.01$.

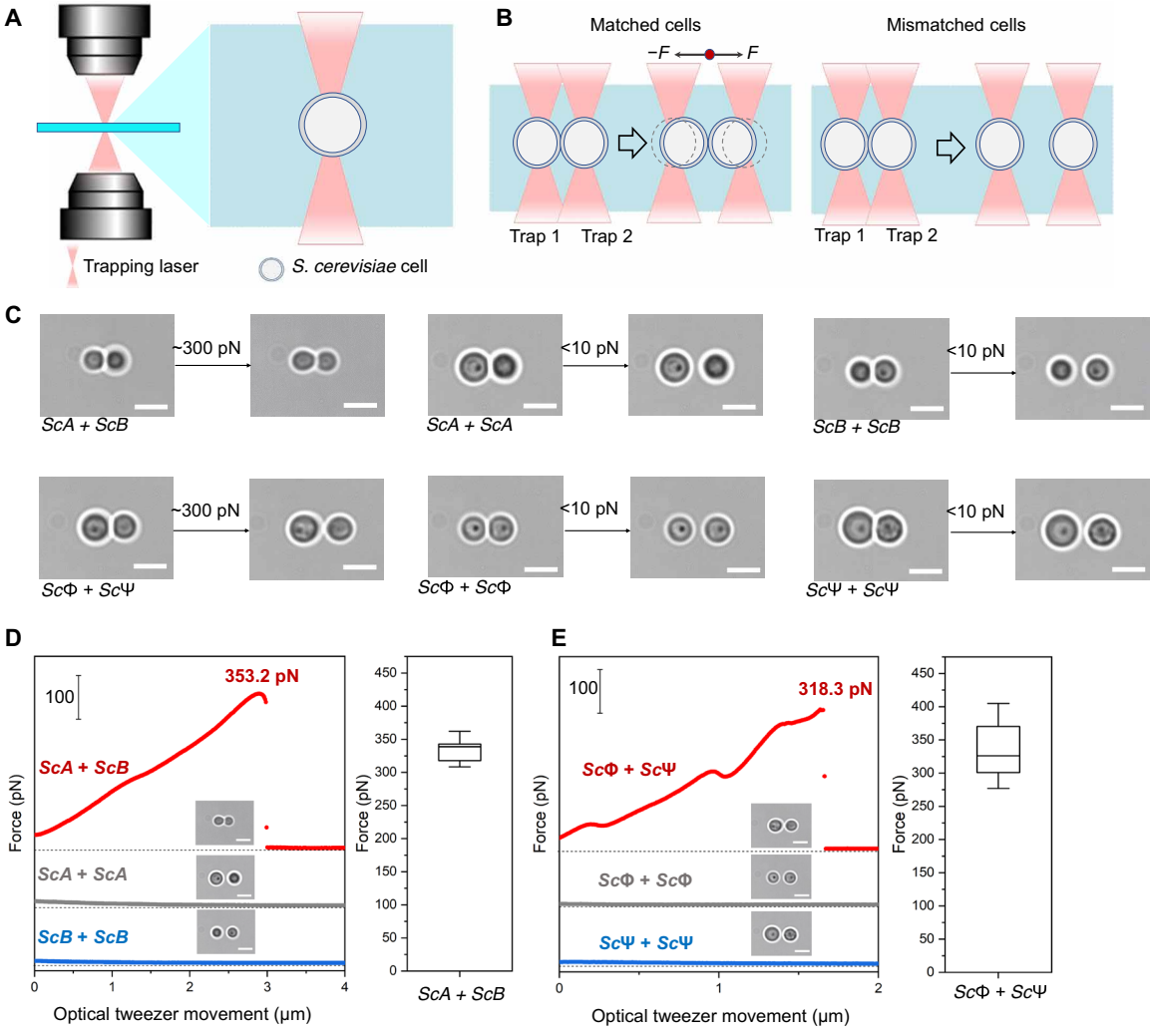

Fig. 4. Cell-to-cell conjugation controlled by optical tweezers. (**A**) Schematic illustration of the trapping of a single cell by an optical tweezer. (**B**) Schematic illustration of the intercellular conjugation and separation by optical tweezers. (**C**) Intercellular conjugation and separation controlled by optical tweezers. Scale bars, 5 μm. (**D** and **E**) Measurement of interaction forces between cells as a function of optical tweezer movement, where Trap 2 was pulled away at a constant velocity (200 nm/s). $n = 10$. Scale bars, 5 μm.

while retaining the assembled structures, the bicellular conjugates that formed via optical trapping served as seeds to be further cultured in the SGCAA medium (Fig. 5A). It turned out that, after 130 h of growth and proliferation, the new cells remained bound to the initial bicellular seeds (*ScA* + *ScB* or *ScΦ* + *ScΨ*), leading to the formation of three-dimensional (3D) multicellular clusters (Fig. 5B). The force measurement with the optical tweezers showed that these multicellular clusters that originated from the matched pairs were remarkably stable; to pull apart the new cells that originated from *ScA* + *ScB* and *ScΦ* + *ScΨ*, considerable forces, up to 248.0 ± 19.2 and 351.4 ± 28.7 pN ($n = 3$), were needed, respectively, substantially larger than those observed among the newly divided cells lacking the complexed SpyTag/SpyCatcher or Im7/CL7 (~36.7 to 133.3 pN), the latter of which might arise from the budding and nonspecific intercellular interactions (Fig. 5, C and D). The marked mechanical stability of these clusters grown out of the paired seeds, *ScA* + *ScB* and *ScΦ* + *ScΨ*, strongly suggests that the designed intercellular PPIs have been not only preserved among the old cells but also inherited by the new ones throughout the growth and proliferation. Moreover, the multicellular structures from the matched pairs exhibited a 3D stacking, relatively compact, while those derived from the mismatched pairs were flat and spread on the bottom of the chamber. These results confirmed that the materials arising from the controlled conjugation of living cells were able to self-propagate and self-assemble while maintaining the compact 3D structures overall as well as the stable intercellular connections. These multicellular ELMs are truly capable of self-propagation, with no need for additional chemical modification, which is therefore superior to traditional polymeric materials or even some other ELM prototypes, the latter of which are often the hybrids of living cells and exogenous polymers (*3*–*8*). These findings also point to a cost-effective approach to future biomaterial manufacturing.

Directed assembly of *S. cerevisiae* via dielectrophoresis

Programmable, long-range assembly of cells, though typical for higher-order organisms, has been rare among the existing ELMs.

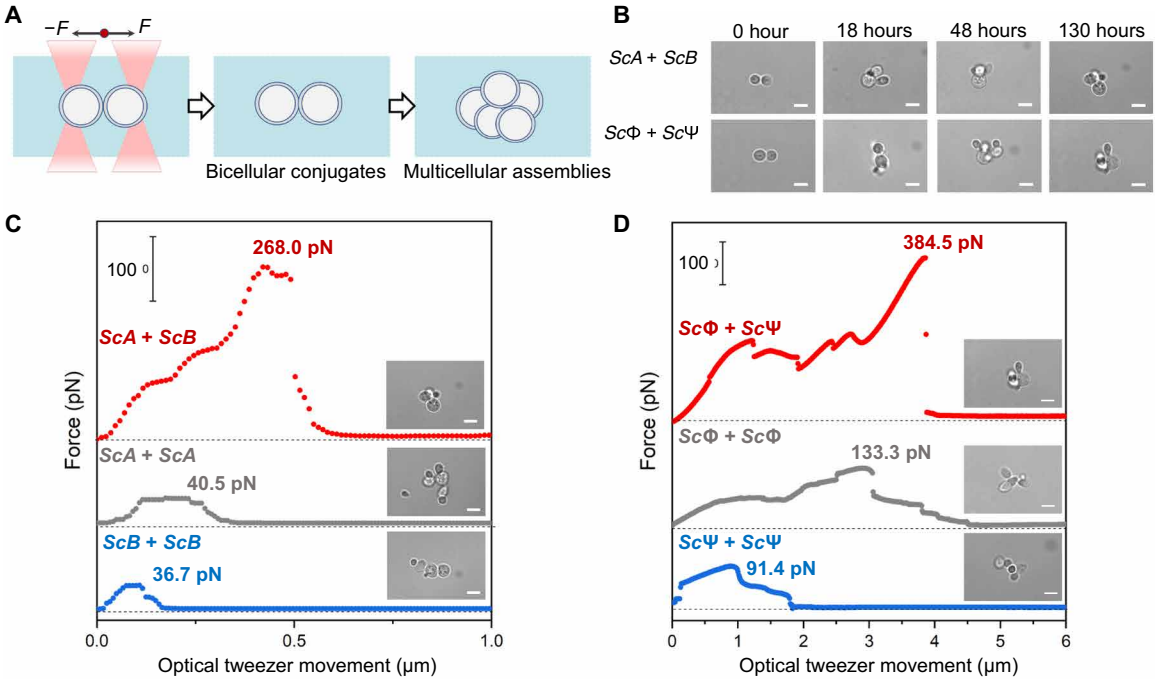

Fig. 5. Growth and proliferation of bicellular conjugates into stable multicellular assemblies. (**A**) Schematic illustration of the creation of a bicellular seed by optical trapping and its subsequent growth into a multicellular structure. (**B**) Growth of initial bicellular seeds into multicellular assemblies via cell proliferation and intercellular conjugation mediated by Spy chemistry or IM7/CL7. Scale bars, 5 μm. (**C** and **D**) Measurement of interaction forces between the new cells, originated from the seeds, *ScA* + *ScB* (C) and *ScΦ* + *ScΨ* (D), as a function of optical tweezer movement, where Trap 2 was pulled away at a constant velocity (200 nm/s). The forces between the mismatched cells were also measured as control. Scale bars, 5 μm.

To control the assembly of *S. cerevisiae* cells, we leveraged dielectrophoresis (DEP), which has been often used in microfluidics to manipulate and assemble dielectric particles and cells (*30*, *31*).

A microdevice was created as described in Methods, which can induce positive DEP (pDEP) and negative DEP (nDEP) via high-frequency (500 kHz to 3 MHz) and low-frequency (3 to 100 kHz) alternating electric fields, respectively (Fig. 6, A and B). To direct the assembly of the cells into ELMs with tailored structures, the doped conductive silicon electrode was patterned with the nonconductive polymer, poly(ethylene glycol) diacrylate (PEGDA), which also had antifouling properties and prevented cell adhesion (fig. S2). pDEP and nDEP were expected to drive the cells to the sites of the maximum and minimum electric field norms, respectively (Fig. 6, A and B). It was confirmed by the respective distributions of the cells on these electrodes at field frequencies of 1 MHz and 100 kHz (Fig. 6C); the cells clustered on the exposed silicon electrodes through pDEP within 10 s but moved away when nDEP was the dominant electrokinetic phenomenon (Fig. 6C). This behavior created the possibility for the formation of stable monodisperse multicellular aggregates or that of a patterned multicellular porous material using PPIs.

To create stable multicellular assemblies from DEP, we mixed the matched cell types, *ScA* + *ScB* and *ScΦ* + *ScΨ*, at a ratio of ~1:1, in the microfluidic device, followed by the introduction of an electric field to generate nDEP. Lattice-like multicellular structures emerged, which remained intact for 1 min for both the *ScA* + *ScB* and *ScΦ* + *ScΨ* pairs after switching from nDEP to pDEP, which generated an opposite dielectrophoretic force (Fig. 6D). By contrast, the mismatched pair, *ScA* + *ScΨ*, assembled via nDEP was transient and fully dissipated 1 min after pDEP was applied (Fig. 6D). These results demonstrated the feasibility of using DEP, alongside the specific intercellular PPIs, to control the assembly of cells into stable, patterned structures.

Multicellular ELMs for uranium extraction

Directly assembling engineered microorganisms into macroscopic living materials, along with their capability of self-propagation and ease of harvesting (compared with single cells), may provide some cost-effective solutions to the challenges facing chemical separation and energy industries, such as uranium extraction from seawater (*32*). There is an enormous uranium reserve (4 billion tons in total) in the ocean—1000 times that on land (*33*). However, large-scale extraction of uranyl (UO_2^{2+}), a major form of oceanic uranium, is extremely challenging because of its very low concentration (~14 nM) and the abundance of competing ions such as calcium, magnesium, and carbonate. On the other hand, unlike other types of heavy metals, which tend to accumulate in the bottom or certain regions of the ocean, uranyl ions are found to be quite evenly distributed across the ocean, regardless of its depth and location (*33*). A variety of synthetic polymeric materials have proved to be feasible for extracting uranium from seawater but at a very high cost (*34*). Developing the ability to tap oceanic uranium in a cost-effective manner will be crucial to our goal of achieving clean energy and sustainable development.

To create functional ELMs capable of uranium extraction, we introduced the gene encoding the super uranyl-binding protein (SUP) (*35*) into the yeast surface display systems, generating two strains, *ScA-SUP* and *ScB-SUP*, which can produce and display

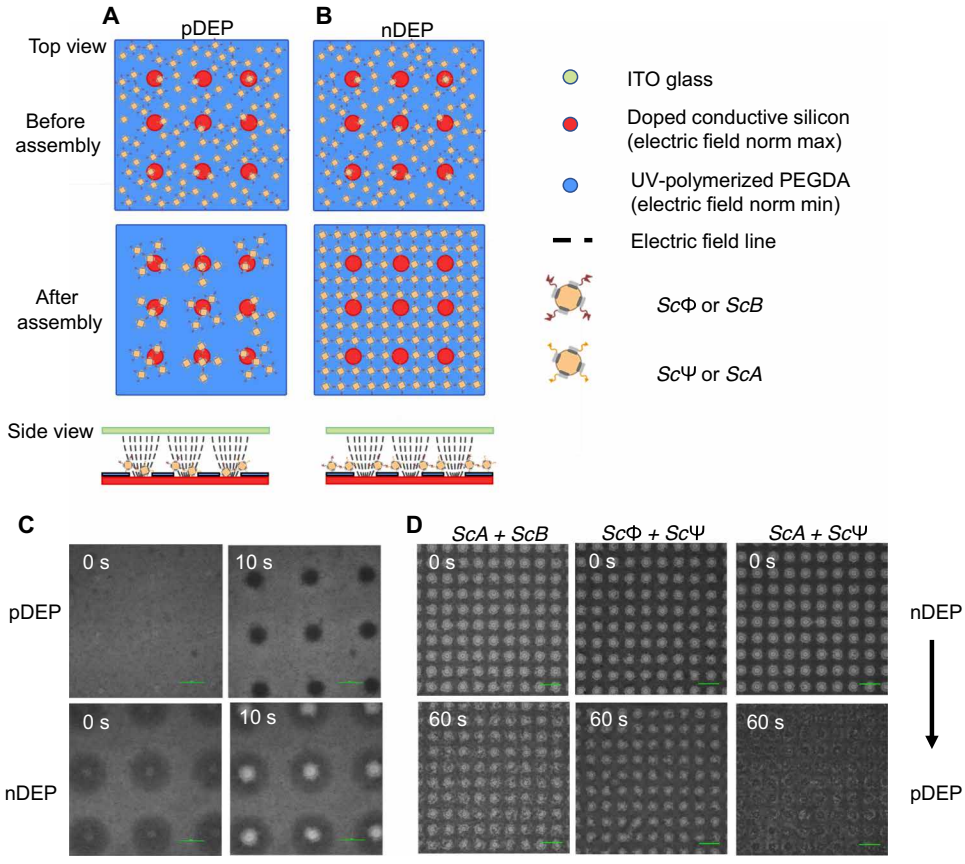

Fig. 6. Directed assembly of yeast cells through DEP. (**A** and **B**) Schematic showing of directed assembly of *S. cerevisiae* by positive DEP (pDEP) (A) and negative DEP (nDEP) (B). UV, ultraviolet; ITO, indium tin oxide; PEGDA, poly(ethylene glycol) diacrylate. (**C**) Micrographs of wild-type yeast cells driven by pDEP and nDEP at 0 and 10 s after applying electric field. Darker shades correspond to the regions with more cells. Scale bars, 100 μm. (**D**) Multicellular assemblies consisting of *ScA* + *ScB* and *ScΦ* + *ScΨ*, induced by nDEP, are stable and resistant toward disruptive dielectrophoretic forces, generated by switching from nDEP to pDEP (1 min). The mismatched pair, *ScA* + *ScΨ*, served as a control. Scale bars, 200 μm.

AGA2-SUP-SpyTag and AGA2-SUP-SpyCatcher, respectively. The introduction of SUP exhibited little effect on the efficiency of the protein surface display, as evidenced by efficient labeling of these cells by the corresponding fluorescent proteins, SpyTag-ELP-EGFP-ELP-SpyTag and SpyCatcher-ELP-EGFP-ELP-SpyCatcher (Fig. 7A and fig. S3). These cells formed clusters upon mixing, which was indicative of the intercellular interactions mediated by SpyTag/SpyCatcher chemistry (Fig. 7A). We further assessed the abilities of these ELMs to extract uranyl, the predominant form of uranium in seawater. It turned out that the yeast cells, even in the absence of SUP, were already able to sequester uranyl, with ~60 to 70% removal from seawater, which might be attributed to the negatively charged glycopeptides on the cell surface (*36*). Introducing SUP further enhanced their efficiency in uranyl sequestration; ~90% uranyl was removed from seawater by the assembled ELM comprising *ScA-SUP* + *ScB-SUP*, and ~89 and ~82% uranyl was removed by the free *ScA-SUP* and *ScB-SUP* cells, respectively (Fig. 7B). Together, these results demonstrated as proof of principle the synthesis of functional ELMs by directly assembling engineered single-celled microorganisms, which might offer an economical approach to energy and environmental issues.

Multicellular ELMs for strengthened mechanics and underwater adhesion

Self-proliferating underwater adhesives can benefit emergency care amid extreme situations such as in a battlefield or a desolate area without basic health care infrastructures and resources. To explore the possibility of developing multicellular assemblies into living adhesives, we introduced into the yeast cells a pair of interacting motifs, mussel foot protein 3/5 (MFP3/5), both of which originated from the marine organism, *Mytilus edulis*, and crucial for its underwater adhesion (*37*, *38*). MFP3 and MFP5 can bind to a variety of substrates in a water-resistant manner (*39*), which is largely attributed to their unique amino acid compositions. They are rich in lysine, a positively charged amino acid, and 3,4-dihydroxyphenylalanine, a posttranslationally modified residue derived from tyrosine oxidation by tyrosinase.

We first examined the cell-to-cell conjugation between the yeast cells, *ScA-MFP3* (red) and *ScA-MFP5* (green), which produce and display AGA2-MFP3-SpyTagand AGA2-MFP5-SpyCatcher, respectively (Fig. 8A and fig. S5). It turned out that the intercellular interactions remained after the introduction of the MFP motifs, as the SpyCatcher- and SpyTag-displaying cells were still able to cluster

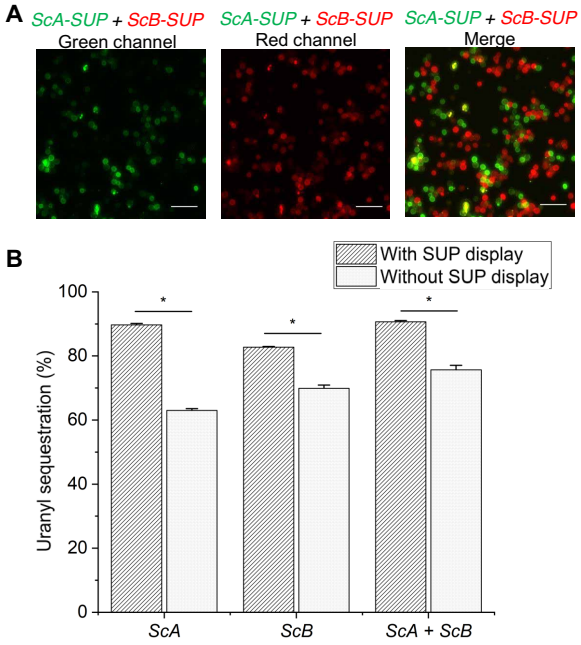

Fig. 7. Multicellular ELMs for uranium extraction. (**A**) Intercellular conjugation of the yeast cells that display SpyTag–super uranyl-binding protein (SUP) (*ScA-SUP*, green) and SpyCatcher-SUP (*ScB-SUP*, red) enabled by SpyTag/SpyCatcher chemistry. The cells, *ScA-SUP* and *ScB-SUP*, were labeled with the SpyCatcher-ELP-Dronpa and SpyTag-ELP-mCherry-ELP-SpyTag proteins, respectively. Scale bars, 25 μm. (**B**) Uranyl extraction from seawater by free and assembled cells. Data are presented as means ± SD ($n = 3$). The two-sample t test was used. *$P < 0.01$.

with each other (Fig. 8A). MFP3 and MFP5 are mechanically strong PPI partners and are responsible for the direct interaction between native mussel foot and underwater substrates. To assess the influence of these domains on the mechanics of ELMs, we performed dynamic rheological tests in frequency and strain sweep modes (Fig. 8, B and C). The ELMs comprising *ScA-MFP5* + *ScB-MFP3* proved to be elastic solids; both, in the presence and absence of tyrosinase, exhibited a steady storage modulus G' of ~10^5 Pa and a loss modulus G'' of ~10^4 Pa over the frequency range of 0.01 to 100 rad/s, substantially higher than those free of MFP3/MFP5, i.e., *ScA* + *ScB* (fig. S6A), suggesting that MFP3 and MFP5 are essential for the observed strong mechanics. Using shear strength adhesive testing, we further assessed the adhesiveness of these multicellular assemblies. The ELM comprising *ScA-MFP5* + *ScB-MFP3* in the presence of tyrosinase proved to be an effective glue on glass and porcine skin (Fig. 8D), generating adhesion strengths of 8.1 ± 2.1 and 8.2 ± 1.5 kPa, respectively, substantially higher than that in the absence of tyrosinase (2.9 ± 1.2 and 2.1 ± 0.7 kPa). This living glue was also stronger than the one free of MFP3/5, i.e., *ScA* + *ScB*, with an adhesive strength of 3.1 ± 0.7 kPa toward porcine skin, suggesting that the presence of the MFP3/5 domains is crucial for strong adhesiveness. On the other hand, either *ScA-MFP5* or *ScB-MFP3* alone turned out to be weaker, even after tyrosinase treatment, in adhesion (~3.0 to 5.0 kPa) than their assembled counterpart, *ScA-MFP5* + *ScB-MFP3*, which suggests that the latter's strong adhesion is likely to be an emergent property out of the combined contributions from the MFP3/5 domains and the multicellular structure (Fig. 8E).

In summary, we have reported a new approach to self-propagating ELMs that involved the use of strong intercellular PPIs to assemble single-celled microorganisms. This assembly process can be precisely controlled in shape and stability via optical tweezers or microfluidics. Depending on the functional motifs introduced by genetic programing, the resulting multicellular ELMs have given rise to emergent properties that hold great promise for applications ranging from uranium extraction to bioadhesion. This study has thus exemplified the use of engineered single cells as versatile building blocks, while free from chemical modification, for synthesizing higher-order living structures or materials. In this sense, this study stands for a new way of thinking for synthetic biology; these single cells are to synthetic biology what atomic/molecular building blocks are to synthetic chemistry.

METHODS

Materials

The pCTcon2 plasmid used for yeast surface display was purchased from Addgene. The genes, including *EGFP*, *mCherry*, *SpyTag*, *SpyCatcher*, *CL7*, and *Im7*, were purchased from Integrated DNA Technologies (table S1). The *MFP3*/*MFP5* genes were ordered from GENEWIZ. The *SUP* gene was obtained as a gift from C. He at the University of Chicago. Uranyl nitrate was purchased from Fisher Scientific, Arsenazo III was from Sigma-Aldrich, and other reagents and all primers were from Sangon Biotech. Seawater was collected by the Coastal Marine Laboratory at the Hong Kong University of Science and Technology (HKUST). The porcine skin was obtained from a local supermarket (ParknShop).

Cloning and plasmid construction

Escherichia coli strain DH5α was used for molecular cloning. The plasmids used for yeast surface display, including pCTcon2-*SpyTag*, pCTcon2-*SpyCatcher*, pCTcon2-*CL7*, and pCTcon2-*Im7*, were constructed by inserting the corresponding genes between Nhe I and Bam HI restriction sites in the pCTcon2 plasmid. Overlapping polymerase chain reaction was used to create fusion genes, including *SUP-SpyTag*, *SUP-SpyCatcher*, *MFP3-SpyTag*, and *MFP5-SpyCatcher*. These genes were then inserted into pCTcon2 using the Nhe I and Bam HI restriction sites. All constructs were verified by Sanger sequencing.

Production and purification of recombinant proteins

E. coli strain BL21 (DE3) was used for protein expression. To produce the fluorescent proteins, the bacterial cells harboring the corresponding plasmids (table S2), pQE80l::*SpyTag-ELP-EGFP-ELP-SpyTag*, pQE80l::*SpyCatcher-ELP-EGFP-ELP-SpyCatcher*, pQE80l::*CL7-ELP-EGFP-ELP-CL7*, pQE80l::*Im7-ELP-EGFP-ELP-Im7*, pQE80l::*SpyCatcher-ELP-Dronpa*, pQE80l::*SpyTag-ELP-mCherry-ELP-SpyTag*, and pQE80l::*Im7-ELP-mCherrry*, were grown in LB at 37°C till the mid-log phase (the optical density at 600 nm or OD_{600} is ~0.6 to 0.8), followed by the addition of 1 mM isopropyl-β-D-thiogalactopyranoside (IPTG; Sangon Biotech) to induce protein expression at 37°C. After 2 hours, the cells were harvested and flash-frozen in liquid nitrogen. The proteins were purified using Ni–nitrilotriacetic acid chromatography following the manufacturer's recommendations (GE Healthcare Inc.). The purified proteins were dialyzed against Milli-Q water (5 liters × 4) at 4°C and lyophilized at −80°C. The resulting protein powders were stored at −80°C before use.

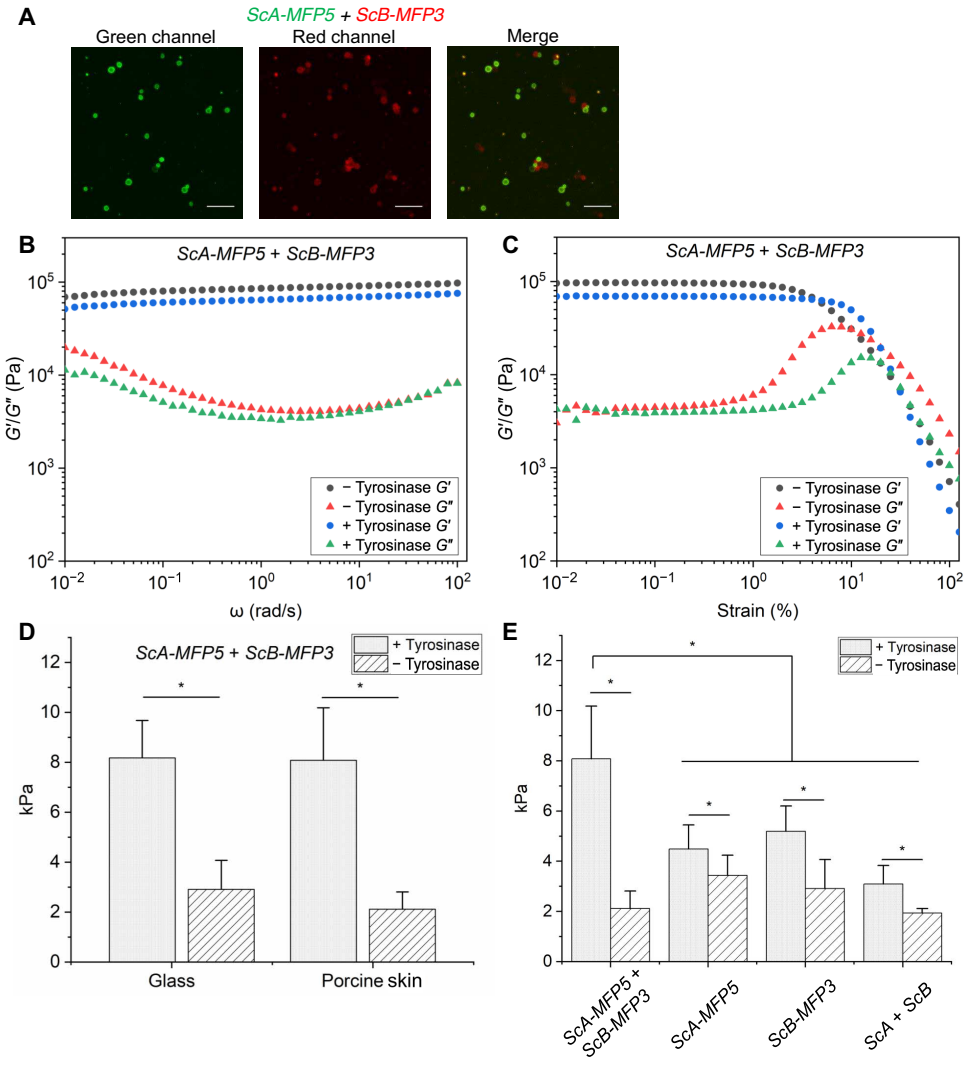

Fig. 8. Strengthened mechanics and underwater adhesion of ELMs by MFP3/5. (**A**) Multicellular assembly of the yeast cells displaying SpyTag-MFP5 (*ScA-MFP5*, green) and SpyCatcher-MFP3 (*ScB-MFP3*, red). *ScA-MFP5* and *ScB-MFP3* cells were labeled by the SpyCatcher-ELP-Dronpa and SpyTag-ELP-mCherry-ELP-SpyTag proteins, respectively. Scale bars, 25 μm. (**B**) Dynamic frequency sweep tests of *ScA-MFP5* + *ScB-MFP3* before and after tyrosinase oxidation. (**C**) Dynamic strain sweep tests of *ScA-MFP5* + *ScB-MFP3* before and after tyrosinase oxidation. (**D**) Adhesion tests of *ScA-MFP5* + *ScB-MFP3* on glass or porcine skin with and without tyrosinase oxidation. (**E**) Adhesion tests of different *S. cerevisiae* cells on porcine skin with and without tyrosinase oxidation. Data are presented as means ± SD ($n = 3$). The two-sample *t* test was used. *$P < 0.01$.

Tyrosinase production and purification

Tyrosinase from *Streptomyces antibioticus* was cloned, expressed, and purified using standard recombinant protein expression methods (*39*). The tyrosinase gene was purchased as gBlocks from Integrated DNA Technologies, cloned into pACYCDuet plasmid, and expressed in *E. coli* BL21(DE3) in TB medium [yeast extract (24 g/liter), tryptone (20 g/liter), glycerol (4 ml/liter), and 0.17 M KH_2PO_4 + 0.72 M K_2HPO_4 (100 ml/liter)]. The *E. coli* cells harboring pACYCDuet-tyrosinase were grown to an OD_{600} of 0.6 to 0.8 and induced with 0.5 mM IPTG at 16°C for 20 hours. The cells were then harvested through centrifugation and resuspended in lysis buffer [300 mM NaCl and 50 mM tris-HCl (pH 8.0)]. The cell suspension was lysed through sonication (Bandelin SONOPULS HD 4400, UW 400, TS113). Proteins were then purified using a 5-ml HisTrap high performance (HP) column (Cytiva Life Sciences) according to the manufacturer's recommendations. Purified tyrosinase was further dialyzed against the dialysis buffer [50 mM sodium phosphate and 0.01 mM $CuSO_4$ (pH 6.5)] at 4°C, diluted to a concentration of 1 mg/ml, flash-frozen with liquid nitrogen, and then stored at −80°C before use.

Yeast surface display

Plasmids were transformed into *S. cerevisiae* EBY100 cells via the lithium acetate method (*40*). The transformants were propagated in the synthetically defined medium with casamino acids (SDCAA) (2% glucose, 0.67% yeast nitrogen base, 0.5% casamino acids, 0.54% Na_2HPO_4, and 0.86% NaH_2PO_4) at 30°C for 14 hours. The yeast cells were induced by replacing SDCAA with SGCAA medium (2% galactose, 0.67% yeast nitrogen base, 0.5% casamino acids, 0.54% Na_2HPO_4, and 0.86% NaH_2PO_4) at room temperature for 24 hours (*41*). The cells were centrifuged (at 9000*g* for 20 s) and resuspended in 1× phosphate-buffered saline (PBS) with a density of 2.0×10^8 cells/ml.

Labeling yeast cells with fluorescent proteins

Cell suspensions (2.0×10^8 cells/ml) and protein solutions (40 mg/ml in PBS) were mixed at a 1:1 volume ratio, with a total volume of 0.1 ml, and then were agitated on a rotator (20 rpm) at room temperature for 1 hour. The cells were spun down and rinsed with 1 ml of PBS three times. The cells were subsequently resuspended with 60 μl of PBS and imaged using a fluorescence microscope (Upright Biological Microscope Ni-U, Nikon, Plan Fluor 40×/0.75 lens).

Cell-to-cell conjugation

The matched two groups of cells (2.0×10^8 cells/ml) were mixed at a roughly 1:1 ratio and then were incubated on a rotator with 20 rpm at room temperature for 1 hour. The cell mixtures were then labeled with fluorescent proteins as described above. The control groups were prepared in the same way.

After assembly and labeling, the cells were diluted by PBS to a density of 4.0×10^7/ml and then imaged under the microscope. At least five images were taken from each sample. Clusters consisting of more than three cells in each image were counted. A confocal microscope (Ni-C2+, Nikon, CFI Plan Apo 10× lens) was used to visualize the resulting cell conjugates.

DEP device fabrication

Device fabrication was conducted in the Nano Fabrication Facility at HKUST. A schematic of the device fabrication process is shown in fig. S1. A silicon wafer was cleaned in the standard Piranha solution and then immersed in the hydrofluoric acid (HF) solution. It was then doped with boron nitride via low-pressure chemical vapor deposition at 950 K for 30 min. The wafer was then subjected to buffered oxide etchant, followed by oxygen plasma at 500 W for 5 min. Surface functionalization was performed immediately after oxygen plasma. The wafer was either (i) preheated to 50°C, spin-coated with silane, and heated for 1 hour or (ii) subjected to vacuum deposition of silane in a vacuum oven at 175°C. The resulting wafer was washed with isopropanol and deionized water, dried with nitrogen, and then cured at 110°C for 30 min. The photocrosslinking solution was made by mixing one part of the saturated Irgacure 369 (the free radical initiator) solution in acetone with nine parts of PEGDA. The photocrosslinking solution was then spin-coated onto the silicon wafer at 1000 rpm for 10 s and 2500 rpm for another 15 s. The wafer, covered with a photomask, was immediately exposed to 365-nm ultraviolet light in an AB-M Aligner for 5 s, subsequently developed in isopropanol for 2 min, and then cured on a 90° to 120°C hotplate.

The patterned wafer was used as a bottom electrode. The bottom electrode was separated from the top electrode (indium tin oxide glass) by a double-sided adhesive silicone rubber spacer (0.5 mm; Grace Bio-Labs), with a 6-mm radius punched hole to load cell suspension.

Directed assembly of *S. cerevisiae* using DEP

Yeast cells were washed with deionized water three times and centrifuged (at 2500*g* for 90 s). The pellets were then resuspended in the solution of 1.6 mM NaCl and 0.1% Triton X-100, with the cell density adjusted to 3.0×10^8 per milliliter. The designated cells, e.g., *ScA* + *ScB*, *ScΦ* + *ScΨ*, etc., were mixed at 1:1 volume ratio and immediately loaded onto the device. The top and bottom electrodes were connected to a function generator to provide AC signal. The assembly process was monitored with a light microscope. DEP experiments were conducted at 10 V at AC frequencies of 3 to 100 kHz and 500 kHz to 3 MHz to induce nDEP and pDEP, respectively.

Force measurement by optical tweezers

Controlled cell-to-cell conjugation was conducted using a dual-trap optical tweezer (m-Trap, LUMICKS). A 1064-nm trapping laser beam was split into two via a polarizing beam splitter and focused inside the sample chamber by a 60× water immersion objective with a 1.2 numerical aperture to trap *S. cerevisiae* cells. A five-channel microfluidic laminar flow chamber was used for the injection, trapping, and conjugation of different types of cells. Two cells were trapped by two trapping laser beams, Trap 1 and Trap 2, respectively. To facilitate intercellular conjugation, one trapped cell (Trap 2) was moved to approach the other (Trap 1). About 10 s after close contact, the Trap 2 cell was pulled away at a constant velocity (200 nm/s), during which the interaction forces were measured. The optical trapping force measurement was calibrated by the built-in force calibration system in the optical tweezer.

In the growth experiment, the bicellular conjugates formed by optical trapping were seeded at the bottom of the microfluidic laminar flow chamber and then cultured in the presence of SGCAA medium at room temperature, during which the trapping lasers were turned off to avoid damaging cells. The growth was monitored using a light microscope. After 130 h of growth, the interaction forces between the cells in the resulting multicellular clusters were measured using optical trapping.

Uranyl extraction from seawater

Free or assembled yeast cells were resuspended in 1 ml of seawater spiked with 500 μM uranyl nitrate and incubated on a rotator (20 rpm) at room temperature for 1 hour. The cells were then pelleted by centrifugation (at 9000*g* for 30 s). The supernatants were diluted by 20-fold in water and then combined with Arsenazo III (80 μM in 0.1 M HCl) at a 1:1 volume ratio. A spectrophotometer (Microplate Reader Varioskan, Thermo Fisher Scientific) was used to determine the remaining uranyl concentration by measuring their absorbance at 652 nm. A standard curve was created to correlate the absorbance at 652 nm with the uranyl concentration (fig. S3).

The percentage of the uranyl ions sequestered by yeast cells was calculated using Eq. 1.

$$\text{percentage of uranyl sequestered} = 100\,\% \times \frac{(C_0 - C_S)}{C_0} \quad (1)$$

where C_0 and C_S are uranyl concentrations in the supernatant before and after the sequestration by yeast cells (*35*, *42*).

Mechanics and adhesiveness of MFP3/5-containing ELMs

After induction, designated yeast cells (1.2×10^9), free or assembled, were resuspended in 10 μl of PBS, supplemented with 1 μg of tyrosinase, and incubated on a rotator (20 rpm) at room temperature for 12 hours. Rheological measurements were performed with 50 μl of ELMs on a TA Instruments ARES-G2 strain-controlled rheometer with a customized steel parallel plate geometry (8 mm in diameter for the upper fixture and 25 mm in diameter for the bottom fixture) at room temperature. Test modes included dynamic strain sweep and frequency sweep. Strain sweep tests were performed over a range of 0.01 to 1000% strain at a fixed frequency of 5 rad/s. Frequency sweep tests were performed from 100 to 0.01 rad/s by holding the strain at 0.1%.

Adhesion tests on glass and porcine skin were performed on the same rheometer. The porcine skin strips (30 mm by 10 mm by 2 mm) were obtained by cropping a piece of cleaned porcine skin. ELMs (7 μl) were applied on the surface (10 by 10 mm^2) of either glass or

porcine skin strips (30 by 10 mm^2) and then placed at 100% relative humidity at room temperature for 3 hours. This prolonged incubation under the humid condition was intended to examine the water resistance of the adhesive ELMs. Tensile tests were performed at a crosshead speed of 0.1 mm/min, and the peak forces were recorded.

SUPPLEMENTARY MATERIALS

Supplementary material for this article is available at https://science.org/doi/10.1126/sciadv.ade0073

View/request a protocol for this paper from *Bio-protocol*.

REFERENCES AND NOTES

1. J. Huang, S. Liu, C. Zhang, X. Wang, J. Pu, F. Ba, S. Xue, H. Ye, T. Zhao, K. Li, Y. Wang, J. Zhang, L. Wang, C. Fan, T. K. Lu, C. Zhong, Programmable and printable *Bacillus subtilis* biofilms as engineered living materials. *Nat. Chem. Biol.* **15**, 34–41 (2019).
2. P. Q. Nguyen, Z. Botyanszki, P. K. Tay, N. S. Joshi, Programmable biofilm-based materials from engineered curli nanofibres. *Nat. Commun.* **5**, 4945 (2014).
3. M. E. Todhunter, N. Y. Jee, A. J. Hughes, M. C. Coyle, A. Cerchiari, J. Farlow, J. C. Garbe, M. A. LaBarge, T. A. Desai, Z. J. Gartner, Programmed synthesis of three-dimensional tissues. *Nat. Methods* **12**, 975–981 (2015).
4. P. J. O'Brien, W. Luo, D. Rogozhnikov, J. Chen, M. N. Yousaf, Spheroid and tissue assembly via click chemistry in microfluidic flow. *Bioconjug. Chem.* **26**, 1939–1949 (2015).
5. K. Nagahama, Y. Kimura, A. Takemoto, Living functional hydrogels generated by bioorthogonal cross-linking reactions of azide-modified cells with alkyne-modified polymers. *Nat. Commun.* **9**, 2195 (2018).
6. T. G. Johnston, S. F. Yuan, J. M. Wagner, X. Yi, A. Saha, P. Smith, A. Nelson, H. S. Alper, Compartmentalized microbes and co-cultures in hydrogels for on-demand bioproduction and preservation. *Nat. Commun.* **11**, 563 (2020).
7. C. Gilbert, T. C. Tang, W. Ott, B. A. Dorr, W. M. Shaw, G. L. Sun, T. K. Lu, T. Ellis, Living materials with programmable functionalities grown from engineered microbial co-cultures. *Nat. Mater.* **20**, 691–700 (2021).
8. L. K. Rivera-Tarazona, T. Shukla, K. A. Singh, A. K. Gaharwar, Z. T. Campbell, T. H. Ware, 4D printing of engineered living materials. *Adv. Funct. Mater.* **32**, 2106843 (2022).
9. M. T. Kozlowski, B. R. Silverman, C. P. Johnstone, D. A. Tirrell, Genetically programmable microbial assembly. *ACS Synth. Biol.*, 1351–1359 (2021).
10. B. Chen, W. Kang, J. Sun, R. Zhu, Y. Yu, A. Xia, M. Yu, M. Wang, J. Han, Y. Chen, L. Teng, Q. Tian, Y. Yu, G. Li, L. You, Z. Liu, Z. Dai, Programmable living assembly of materials by bacterial adhesion. *Nat. Chem. Biol.* **18**, 289–294 (2022).
11. J. Fang, A. Mehlich, N. Koga, J. Huang, R. Koga, X. Gao, C. Hu, C. Jin, M. Rief, J. Kast, D. Baker, H. Li, Forced protein unfolding leads to highly elastic and tough protein hydrogels. *Nat. Commun.* **4**, 2974 (2013).
12. X. Liu, X. Yang, Z. Yang, J. Luo, X. Tian, K. Liu, S. Kou, F. Sun, Versatile engineered protein hydrogels enabling decoupled mechanical and biochemical tuning for cell adhesion and neurite growth. *ACS Appl. Nano Mater.* **1**, 1579–1585 (2018).
13. B. M. Park, J. Luo, F. Sun, Enzymatic assembly of adhesive molecular networks with sequence-dependent mechanical properties inspired by mussel foot proteins. *Polym. Chem.* **10**, 823–826 (2019).
14. F. Sun, W. B. Zhang, A. Mahdavi, F. H. Arnold, D. A. Tirrell, Synthesis of bioactive protein hydrogels by genetically encoded SpyTag-SpyCatcher chemistry. *Proc. Natl. Acad. Sci. U.S.A.* **111**, 11269–11274 (2014).
15. R. Wang, Z. Yang, J. Luo, I. M. Hsing, F. Sun, B12-dependent photoresponsive protein hydrogels for controlled stem cell/protein release. *Proc. Natl. Acad. Sci. U.S.A.* **114**, 5912–5917 (2017).
16. J. Wu, P. Li, C. Dong, H. Jiang, X. Bin, X. Gao, M. Qin, W. Wang, C. Bin, Y. Cao, Rationally designed synthetic protein hydrogels with predictable mechanical properties. *Nat. Commun.* **9**, 620 (2018).
17. Z. Yang, S. Kou, X. Wei, F. Zhang, F. Li, X.-W. Wang, Y. Lin, C. Wan, W.-B. Zhang, F. Sun, Genetically programming stress-relaxation behavior in entirely protein-based molecular networks. *ACS Macro Lett.* **7**, 1468–1474 (2018).
18. H. J. Kang, F. Coulibaly, F. Clow, T. Proft, E. N. Baker, Stabilizing isopeptide bonds revealed in Gram-positive bacterial pilus structure. *Science* **318**, 1625–1628 (2007).
19. L. Li, J. O. Fierer, T. A. Rapoport, M. Howarth, Structural analysis and optimization of the covalent association between SpyCatcher and a peptide tag. *J. Mol. Biol.* **426**, 309–317 (2014).
20. C. T. S. Wong Po Foo, J. S. Lee, W. Mulyasasmita, A. Parisi-Amon, S. C. Heilshorn, Two-component protein-engineered physical hydrogels for cell encapsulation. *Proc. Natl. Acad. Sci. U.S.A.* **106**, 22067–22072 (2009).
21. L. Liu, J. A. Shadish, C. K. Arakawa, K. Shi, J. Davis, C. A. DeForest, Cyclic stiffness modulation of cell-laden protein–polymer hydrogels in response to user-specified stimuli including light. *Adv. Biosyst.* **2**, 1800240 (2018).
22. H. Feldmann, *Yeast: Molecular and Cell Biology* (Wiley-VCH Hoboken, 2013).
23. E. T. Boder, K. D. Wittrup, Yeast surface display for screening combinatorial polypeptide libraries. *Nat. Biotechnol.* **15**, 553–557 (1997).
24. G. Chao, W. L. Lau, B. J. Hackel, S. L. Sazinsky, S. M. Lippow, K. D. Wittrup, Isolating and engineering human antibodies using yeast surface display. *Nat. Protoc.* **1**, 755–768 (2006).
25. H. Zhang, K. K. Liu, Optical tweezers for single cells. *J. R. Soc. Interface* **5**, 671–690 (2008).
26. W. X. Sun, X. Gao, H. Lei, W. Wang, Y. Cao, Biophysical approaches for applying and measuring biological forces. *Adv. Sci.* **9**, 2105254 (2022).
27. A. J. Crick, M. Theron, T. Tiffert, V. L. Lew, P. Cicuta, J. C. Rayner, Quantitation of malaria parasite-erythrocyte cell-cell interactions using optical tweezers. *Biophys. J.* **107**, 846–853 (2014).
28. X. Gou, R. Wang, S. S. Y. Lam, J. D. Hou, A. Y. H. Leung, D. Sun, Cell adhesion manipulation through single cell assembly for characterization of initial cell-to-cell interaction. *Biomed. Eng. Online* **14**, 114 (2015).
29. E. Fallman, S. Schedin, J. Jass, M. Andersson, B. E. Uhlin, O. Axner, Optical tweezers based force measurement system for quantitating binding interactions: System design and application for the study of bacterial adhesion. *Biosens. Bioelectron.* **19**, 1429–1437 (2004).
30. J. Oh, R. Hart, J. Capurro, H. Noh, Comprehensive analysis of particle motion under non-uniform AC electric fields in a microchannel. *Lab Chip* **9**, 62–78 (2009).
31. K. H. Bhatt, S. Grego, O. D. Velev, An AC electrokinetic technique for collection and concentration of particles and cells on patterned electrodes. *Langmuir* **21**, 6603–6612 (2005).
32. F. Sun, C. He, Reaction: Engineer biology for uranium. *Chem* **7**, 274–275 (2021).
33. Y. Nozaki, A fresh look at element distribution in the North Pacific Ocean (EOS, Transactions American Geophysical Union, 1997).
34. C. J. Leggett, F. Endrizzi, L. F. Rao, Scientific basis for efficient extraction of uranium from seawater, II: Fundamental thermodynamic and structural studies. *Ind. Eng. Chem. Res.* **55**, 4257–4263 (2016).
35. L. Zhou, M. Bosscher, C. S. Zhang, S. Ozcubukcu, L. Zhang, W. Zhang, C. J. Li, J. Z. Liu, M. P. Jensen, L. H. Lai, C. He, A protein engineered to bind uranyl selectively and with femtomolar affinity. *Nat. Chem.* **6**, 236–241 (2014).
36. S. M. Tazhibaeva, K. B. Musabekov, A. B. Orazymbetova, A. A. Zhubanova, Surface properties of yeast cells. *Colloid J.* **65**, 122–124 (2003).
37. Q. Y. Lu, E. Danner, J. H. Waite, J. N. Israelachvili, H. B. Zeng, D. S. Hwang, Adhesion of mussel foot proteins to different substrate surfaces. *J. R. Soc. Interface* **10**, 20120759 (2013).
38. B. P. Lee, P. B. Messersmith, J. N. Israelachvili, J. H. Waite, Mussel-inspired adhesives and coatings. *Annu. Rev. Mat. Res.* **41**, 99–132 (2011).
39. J. Luo, X. Liu, Z. Yang, F. Sun, Synthesis of entirely protein-based hydrogels by enzymatic oxidation enabling water-resistant bioadhesion and stem cell encapsulation. *ACS Appl. Bio Mater.* **1**, 1735–1740 (2018).
40. R. D. Gietz, R. H. Schiestl, High-efficiency yeast transformation using the LiAc/SS carrier DNA/PEG method. *Nat. Protoc.* **2**, 31–34 (2007).
41. I. Chen, B. M. Dorr, D. R. Liu, A general strategy for the evolution of bond-forming enzymes using yeast display. *Proc. Natl. Acad. Sci. U.S.A.* **108**, 11399–11404 (2011).
42. S. Z. Kou, Z. G. Yang, F. Sun, Protein hydrogel microbeads for selective uranium mining from seawater. *ACS Appl. Mater. Interfaces* **9**, 2035–2039 (2017).

Acknowledgments

Funding: The funding support from the Ministry of Science and Technology to F.S. (2020YFA0908100); from Natural Science Foundation of China Excellent Young Scientists Fund to F.S. (22122707), from the Science, Technology, and Innovation Commission of Shenzhen Municipality to F.S. [Key Research Program no. JCYJ20200109141241950, Shenzhen-Hong Kong-Macau S&T Program (Category C) no. SGDX2020110309460101, and Basic Research Program no. JCYJ20190813094601656]; from Guangdong Provincial Natural Science Foundation to F.S. (2019A1515011691); and from the Research Grants Council of Hong Kong SAR Government to F.S. (GRF grants no. 16103519 and no.16103421; Theme-based Research Scheme no. T13-602/21-N), from the State Key Laboratory of Molecular Neuroscience, HKUST, China, and in part from the Innovation and Technology Commission (ITCPD/17-9) is acknowledged. **Author contributions:** F.S. conceived the idea. F.S., R.L., and J.H. conceived the design and supervised the study. Q.Y., X.D., B.M.P., J.G., J.L., R.W., S.K., J.H., and F.S. designed and performed the experiments. Q.Y., X.D., B.M.P., J.G., C.Y., S.K., J.H., R.L., and F.S. analyzed data and wrote the manuscript. All authors reviewed and provided inputs on the manuscript. **Competing interests:** The authors declare that they have no competing interests. **Data and materials availability:** All data needed to evaluate the conclusions in the paper are present in the paper and/or the Supplementary Materials.

Submitted 19 July 2022
Accepted 17 September 2022
Published 4 November 2022
10.1126/sciadv.ade0073